Biochemistry

 Volume 20, Number 9 April 28, 1981

Crystallographic Refinement and Atomic Models of a Human Fc Fragment and Its Complex with Fragment B of Protein A from *Staphylococcus aureus* at 2.9- and 2.8-Å Resolution†

Johann Deisenhofer

ABSTRACT: The model of human Fc fragment was refined at 2.9-Å resolution. Two different automated procedures for crystallographic refinement were used [Deisenhofer, J., & Steigemann, W. (1975) *Acta Crystallogr., Sect. B B31*, 238; Jack, A., & Levitt, M. (1978) *Acta Crystallogr., Sect. A A34*, 931]. The final R value is 0.22. The dimer of CH3 domains closely resembles the CH1–CL aggregate in Fab fragments. There is no contact between CH2 domains. The contact between CH2 and CH3 domains has about one-third of the size of the CH3–CH3 contact. The carbohydrate, a branched chain of nine hexose units, covers part of the C-contact face of the CH2 domain, shielding hydrophobic residues on this surface. Six atoms of the carbohydrate are within hydrogen-bonding distance of atoms in the CH2 domain. Crystallographic refinement of the complex between Fc fragment and fragment B of protein A from *Staphylococcus aureus* reduced the R value of the model to 0.24. A major part of the structure of fragment B consists of two α helices; the rest of the polypeptide chain is folded irregularly. In the crystal, fragment B forms two contacts with Fc fragment molecules. Contact 1 involves residues from both helices of fragment B, and residues from the CH2 and CH3 domains of Fc, and is predominantly hydrophobic. Contact 2 is smaller than contact 1. Residues from the second helix and adjacent residues of fragment B and residues only from the CH3 domain of Fc contribute to contact 2. The nature of contact 2 is mainly polar and includes a sulfate ion. There are strong arguments that contact 1 is the fragment B–Fc contact formed in solution under physiological conditions, while contact 2 is a crystal contact.

The Fc fragment of an immunoglobulin molecule is the dimer of the two C-terminal constant-homology regions of the heavy chain. Among its physiological functions are interactions with the complement system and with specific receptors on the surface of a variety of cells.

The crystal structure of an IgG Fc fragment, obtained from pooled human serum, was studied at 4- (Deisenhofer et al., 1976a) and at 3.5-Å resolution (Deisenhofer et al., 1976b) with the method of multiple isomorphous replacement. These studies revealed the quaternary structure of the molecule and the location of the carbohydrate moiety, which is covalently attached to the CH2 domain. The folding of the polypeptide chain was described on the basis of a preliminary atomic model.

Protein A is a constituent of the cell wall of *Staphylococcus aureus*. Part of its polypeptide chain is a series of four highly homologous regions (Sjodahl, 1977), each of which is able to bind to the Fc part of IgG from various species. Protein A is widely used as a tool in immunochemical and related studies. Its biological role is unknown.

The crystal structure of the complex formed by human Fc fragment and fragment B of protein A was solved by using multiple isomorphous replacement and the known model of the Fc fragment (Deisenhofer et al., 1978). The binding site of FB[1] to Fc fragment and the tertiary structure of FB in the complex was described.

For improvement of both models, the Fc fragment and the FB–Fc complex, and to allow a more detailed description, a crystallographic refinement was done. In this paper I describe the crystallographic refinement and the resulting refined models of the Fc fragment and the FB–Fc complex.

Experimental Methods

Crystal Data. The human Fc fragment crystallizes in space group $P2_12_12_1$ with unit cell dimensions of a = 80.4, b = 146.4, and c = 50.4 Å. There is one Fc fragment molecule in the asymmetric unit (Deisenhofer et al., 1976a). X-ray intensity data were collected by film methods using screenless precession and rotation techniques. For the native data set, 76 films, taken from 23 crystals, were evaluated as described by

† From the Max-Planck-Institut fuer Biochemie, D-8033 Martinsried, West Germany. *Received September 22, 1980.*

[1] Abbreviations used: mir, multiple isomorphous replacement; rms, root mean square; F_{obsd}, observed structure factor; F_{calcd}, calculated structure factor; α_{calcd}, calculated phase angle; B, temperature factor; Fab, antigen-binding fragment consisting of light chain and the N-terminal half of the heavy chain; FB, fragment B of protein A; Fc, C-terminal half of the heavy chain with the inter-heavy-chain disulfide bond intact; CH1, CH2, and CH3, the constant homology regions of the heavy chain; hinge peptide, the segment connecting CH1 and CH2 and containing the disulfide linkage between the two heavy chains; C face, the face on a C domain that is involved in the C–C type aggregation.

0006-2960/81/0420-2361$01.25/0

Schwager et al. (1975). Significant intensities were measured for 48 829 observations of 10 342 independent reflections to 2.9-Å resolution. This is 75% of the total number of reflections in this resolution range; between 3.0- and 2.9-Å resolution, the fraction of significantly measured intensities was 37%. Data from individual films were merged together and scaled by using the method and program of Steigemann (1974). After this procedure, R_{scale} was 0.077

$$R_{scale} = \sum|I(i) - \langle I\rangle|/I(i)$$

[$I(i)$ is the intensity value of an individual measurement, and $\langle I\rangle$ is the corresponding mean value; the summation is over all measurements].

The crystals of the FB–Fc complex belong to space group $P3_121$; the unit cell dimensions are $a = b = 70.6$ Å and $c = 147.4$ Å. The complex lies on a crystallographic diad; thus, the asymmetric unit contains one CH2 domain, one CH3 domain, and one B fragment from protein A. Evaluation of 41 films for 11 crystals yielded 25 876 significant reflection intensities for 7002 unique reflections to 2.8-Å resolution with $R_{scale} = 0.079$. This is 62% of the total number of reflections. The intensities of 3626 independent reflections were below the significance level.

Starting Models. The starting model for crystallographic refinement of the Fc fragment was obtained as described by Deisenhofer et al. (1976b): An electron-density map at 3.5-Å resolution was calculated with phases from multiple isomorphous replacement. By use of an optical comparator, wire models of one CH2 domain and one CH3 domain, both belonging to chain 1, were built on the basis of the amino acid sequence of the human myeloma protein Eu (Rutishauser et al., 1970). Atomic coordinates read from the model were idealized with Diamond's (Diamond, 1966) model building procedure; the fit to the electron density was improved by Diamond's (Diamond, 1971) real-space refinement procedure. The branched carbohydrate chain attached to the CH2 domain was built in three segments by using known hexose geometry. One segment consisted of five hexose units and the other two of two hexose units each; the links between the segments remained uncertain. After generation of coordinates for chain 2 of the Fc fragment by using the known local symmetry and performance of additional rigid-body refinement and real-space refinement, structure factors were calculated with the coordinates of 2788 well-defined atoms from residues Pro-238 to Ser-442 in both chains. An overall temperature factor of 21.3 Å^2 was used as determined from a Wilson plot. The R value for all data between 5- and 2.9-Å resolution was 0.44 ($R = \sum||F_{obsd}| - |F_{calcd}||/\sum|F_{obsd}|$).

The starting model for refinement of the FB–Fc–complex was based on an electron-density map calculated with mir phases at 3.5-Å resolution (Deisenhofer et al., 1978). One CH2 domain and one CH3 domain from a partially refined Fc fragment model (stage 8) were fitted to the density by rigid-body transformation. Electron density was missing for about one-third of the CH2 domain. The protein A fragment model was built with a graphics display system using an electron-density map calculated with combined mir and Fc fragment model phases at 2.8-Å resolution.

Crystallographic Refinement. Two different methods of cyclic crystallographic refinement were used. Part 1 of the refinement began with the method described by Deisenhofer & Steigemann (1975). One refinement cycle included calculation of structure factors from model atomic coordinates, calculation of an electron-density map by using data with Bragg spacings between 7 and 2.9 Å with the coefficients $(n|F_{obsd}| - (n-1)|F_{calcd}|)\exp(i\alpha_{calcd})$, $1 \le n \le 3$, and fitting of the model to this map with Diamond's (Diamond, 1971, 1974) real-space refinement procedure. The resulting coordinates were used as input for the next cycle of refinement. The electron-density maps were calculated with a grid spacing of 0.9 Å. Reflections with $2||F_{obsd}| - |F_{calcd}||/(|F_{obsd}| + |F_{calcd}|) > 1.2$ were omitted from Fourier summation. The real-space refinement procedure works with fixed values for bond lengths, most bond angles, and some torsion angles. A "molten zone" of between 2 and 10 residues slides along the chain; only atoms within the molten zone can move. In the study described here, the length of the molten zone was 6 residues. The φ and ψ torsion angles of the main chain and torsion angles $\chi_1 - \chi_4$ of the side chains were flexible. Flexible $\tau(N–C^\alpha–C)$ bond angles were introduced in an advanced stage of the refinement. Due to the low resolution of the data, real-space refinement produced a number of close interatomic contacts. These bad contacts were removed with an energy-refinement program (Levitt & Lifson, 1969; Levitt, 1974).

In part 2 of the refinement, the method of Jack & Levitt (1978) was used instead of real-space refinement. This method derives the normal equations for a diagonal-matrix least-squares refinement from a difference-Fourier map. The crystallographic residual $\sum(|F_{obsd}| - |F_{calcd}|)^2$ is then minimized together with the conformational energy of the model. The relative weights of crystallographic residual and conformational energy can be set through a scale factor. The value of this scale factor decides whether idealized model geometry is strictly kept or relaxed in favor of a smaller crystallographic residual. Energy parameters for bond lengths, bond angles, torsion angles, and nonbonded interactions were those recommended by Levitt (1974), except that proline rings were kept flat with torsion-angel potentials similar to the ones used for aromatic rings. Difference-Fourier maps were calculated with grid spacings of one-third of the resolution limit. The resolution range varied between 7–4 Å and 7–2.9 Å.

The diagonal-matrix least-squares method was also used to refine isotropic temperature factors. Individual B values of the atoms of each residue were averaged to give one B value per residue.

Typically, the automated refinement reached a local minimum of crystallographic R value after about four cycles of either procedure, at which point the errors remaining in the model required shifts of atomic coordinates greater than the radius of convergence of the refinement method in use. In order to detect such errors and to get an idea of the necessary corrections, I carried out the following steps: In part 1 of the refinement, difference-Fourier maps were calculated and plotted on paper along with the model atomic coordinates. Corrections to the model deduced from the map were applied either with an option of the real-space refinement program, which allows input of desired values for torsion angles or atomic positions which the program then tries to realize, or with Diamond's model-building program.

In part 2 of refinement, inspection of maps and modifications of the model were significantly simplified by the use of an interactive graphics display system. The most helpful features of this system, programmed by Jones (1978), are rotation around bonds, shifting of atoms or atom groups, and changes of the chemical sequence. If necessary, ideal geometry can be restored after such operations with a modified version of the model-building program of Hermans & McQueen (1974). Maps calculated with coefficients $2|F_{obsd}| - |F_{calcd}|$ and either model phases, Sim-weighted model phases (Hendrickson & Lattman, 1970), or phases resulting from combination of model phases and mir phases (Hendrickson & Lattman, 1970)

were used with the display. In the phase combination procedure, model phases and mir phases were given equal weights. Structure factors, R values, and electron-density maps were calculated with Steigemann's "PROTEIN" program system (Steigemann, 1974). The refinement of the FB–Fc complex was done in parallel with Fc fragment refinement by using identical methods.

Accessible Surface Areas and Hydrogen Bonds. The various interdomain contacts in Fc fragment and FB–Fc complex were investigated by calculating and comparing the accessible surface areas of separate domains and composite molecules. A computer program, based on the method of Lee & Richards (1971) and written by Levitt (personal communication; Chothia, 1975), was used for these calculations. The probe size, i.e., the radius of a water molecule, was set to 1.4 Å. The method assumes the molecules to be rigid. Atoms which are mobile in the crystal were included in the calculations.

A second option of Levitt's program was used to search for hydrogen bonds. The proposed hydrogen bond candidates with a donor–acceptor distance of <3.5 Å were checked by eye at the display system to see whether they approximately met the geometric requirements for hydrogen-bond formation.

Amino Acid Sequence Homologies. For comparison of amino acid sequences of different domains and antibody molecules, the table composed by Beale & Feinstein (1976) was used.

Results and Discussion

Crystallographic Refinement of Fc Fragment. The course of Fc fragment refinement part 1 (Diamond refinement) and part 2 (Jack–Levitt refinement) is listed in Tables Ia and Ib (see paragraph at end of paper regarding supplementary material). On the average, four cycles of automated refinement were carried out between calculation of the maps.

Between the start of refinement and step 3, the second difference-Fourier map, the R value was reduced by 0.06. Between steps 3 and 7, R decreased very slowly. The introduction of free $\tau(N–C^{\alpha}–C)$ angles resulted in a larger decrease of R between steps 7 and 8. After step 8, the Jack–Levitt refinement was begun with an initial scale factor between crystallographic residual and conformational energy of 10^{-4}; this scale factor was later decreased to 3×10^{-5}. The large decrease of R between steps 8 and 9 [Table Ib (supplementary material)] was at least in part due to relaxation of geometric constraints, which led to a high energy of the model. Between steps 9 and 11, mainly the energy was lowered at constant R. In the final steps 11–15, further corrections of the model reduced both R and the conformational energy. In steps 9–15, whenever large manual changes of the model were done, subsequent automated refinement was started at 7–4-Å resolution to increase the radius of convergence (Jack & Levitt, 1978). In the following cycles, the upper resolution limit was gradually increased to 2.9 Å. The refinement converged at an R-value of 0.22 for reflections between 7- and 2.9-Å resolution.

Average residue temperature factors were updated before inspection of each new map. When individual B values were averaged, the minimum allowed value was set to 6 Å^2.

Due to the low resolution, the difference-Fourier maps were difficult to interpret. In many cases, incorrect parts of the model could be recognized clearly from negative density; the corresponding positive density which indicates the correct atomic positions was often rather weak and difficult to interpret. The situation was not improved when atoms with uncertain positions were left out of the structure factor calculation. The interpretation of the $2|F_{obsd}| - |F_{calcd}|$ maps was found less difficult. Electron density for many of the atoms with uncertain positions, which were left out from the structure factor calculation, could be found. In cases where the model did not coincide with the electron density, it was possible to try different model conformations in search of a better fit. The $2|F_{obsd}| - |F_{calcd}|$ maps calculated with combined model and mir phases provided the clearest guide to necessary changes in the model. Phase combination also allowed inclusion of low-resolution reflections (those with Bragg spacings >7 Å) in the Fourier summation. As with most refined protein structures, the fit between observed and calculated structure factors at low resolution is very poor; for this reason, model phases of reflections inside the 7-Å sphere were not used except in combination with mir phases.

In general, corrections to the model made "by hand" were influenced by the inspected map, by stereochemical considerations (plausible conformation, contacts to neighbors), and by comparison of the two crystallographically independent polypeptide chains of the Fc fragment molecule. On several occasions, polypeptide segments of up to five residues were deliberately built with different conformation in both chains to see which one would fit better to the electron density after the next cycles of automated refinement. The mir map was used throughout the refinement of the Fc fragment as an additional guide when the model was changed. After each round of manual corrections to the model, the R value rose by 0.01–0.03; the first one or two cycles of automated refinement were needed to bring R back to the previous level.

Observed structure factor amplitudes of 9332 reflections between 7- and 2.9-Å resolution were used for refinement. During real-space refinement, 2092 conformational angles were flexible parameters. The number of free parameters in Jack–Levitt refinement is more difficult to count, because the relative weight of crystallographic and energy contributions depends on the choice of the scale factor. A total of 10 596 coordinates of 3532 atoms (of which only 3182 contributed to calculated structure factors during the final cycles) were restrained by 3646 bond lengths, 4998 bond angles, and 6072 torsion angle potentials. A total of 1598 torsion angles had energy barriers of 20 kcal/mol or more. About 40 000 atom pairs with distances less than the sum of the van der Waals radii plus 2.0 Å contributed to the nonbonded interaction energy; pairs of atoms which occur in a bond, a bond angle, or a torsion angle were excluded from the list of nonbonded interactions.

During this work, the following main advantages of the Jack–Levitt refinement method were noticed: (a) refinement at low resolution is possible, (b) geometric restraints can be relaxed temporarily, (c) treatment of branched chains is easy, (d) the method requires ~30% less computing time than Diamond's real-space refinement, (e) distorted geometry can be repaired, and (f) refinement of temperature factors at 2.9-Å resolution is possible.

The rms difference between C^{α} coordinates of chain 1 of the starting and refined models is 1.18 Å for 158 of the 206 residues. This value is very large compared to the rms C^{α} shift of 0.45 Å during refinement of the pancreatic trypsin inhibitor (Deisenhofer & Steigemann, 1975), where the initial model was based on a mir map at 1.9-Å resolution.

In each polypeptide chain 38 residues and the carbohydrate moiety had to be rebuilt during refinement. These residues belong to segments Val-284 to His-310, Pro-353 to Met-358, Asn-384 to Asn-390, Gly-402, Glu-430 to His-435, and Leu-443, which was not present in the starting model. For residues 385–389, the amino acid sequence was changed from

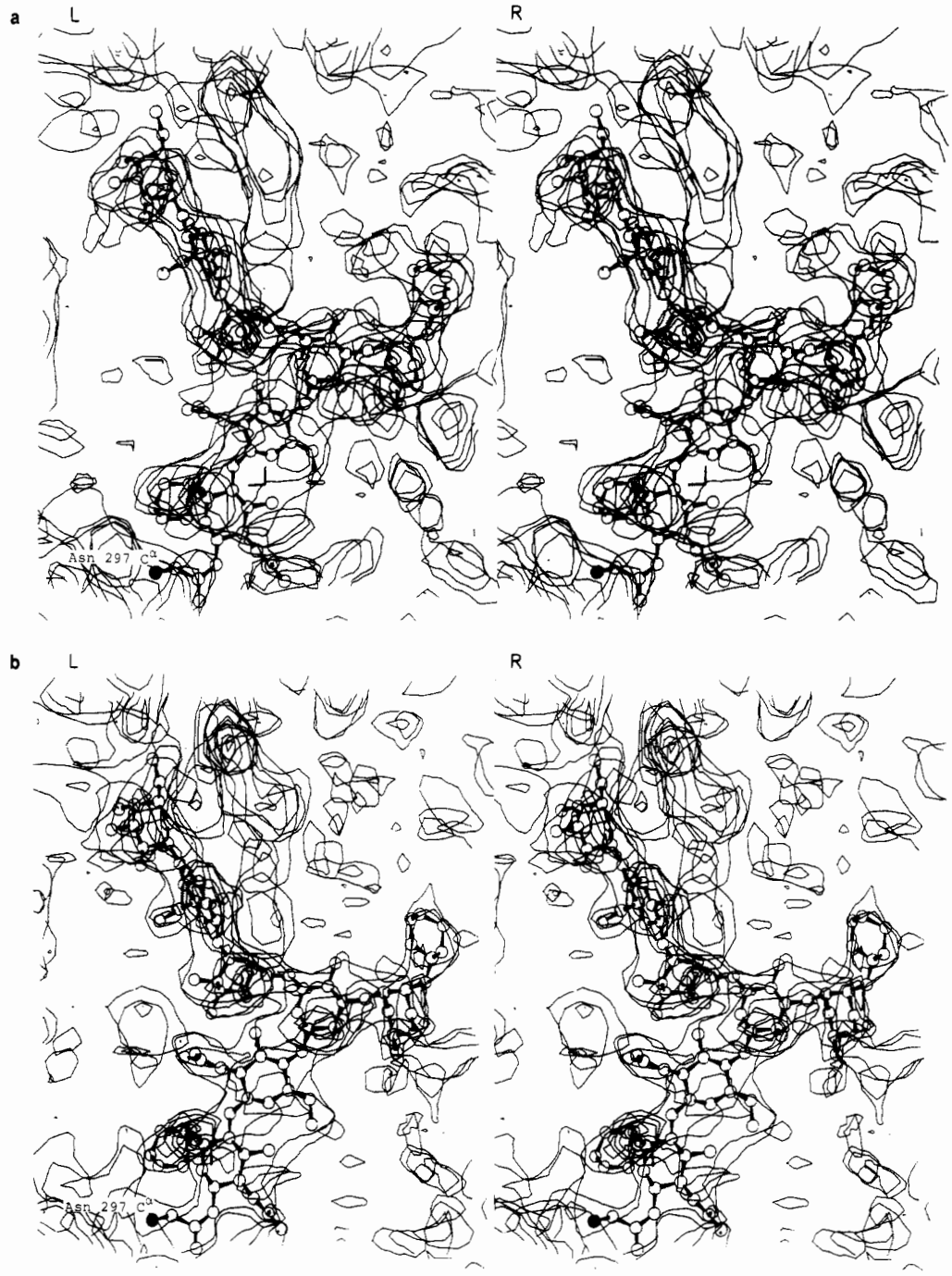

FIGURE 1: Stereo drawings of refined model of carbohydrate and side chain of Asn-297 (only atoms contributing to F_{calcd}): (a) the mir map (3.5-Å resolution; contour levels at 0.17 and 0.51 e/Å^3) and (b) the final $2|F_{obsd}| - |F_{calcd}|$ map (2.9-Å resolution; combined mir and model phases; contour levels at 0.25 and 0.75 e/Å^3). Parts of the electron density belong to the protein; the corresponding model was omitted.

Asp-Gly-Glu-Pro-Glu to Gly-Gln-Pro-Glu-Asn (Ponstingl & Hilschmann, 1972; Hofmann & Parr, 1979). Only the later amino acid sequence is compatible with the electron density. No interpretable electron density could be found for residues Thr-223 to Gly-237, which include almost the whole hinge region with the inter-heavy-chain disulfide bridges. At the C-terminal end, residues 444–446 remained undefined. The carbohydrate model includes 9 of the 12 possible hexose units (Kornfeld & Kornfeld, 1976). Figure 1 shows for comparison the refined carbohydrate model (chain 1) drawn into both the mir map and the final $2|F_{obsd}| - |F_{calcd}|$ map calculated with combined phases.

The average temperature factor in both CH3 domains is 19.5 Å^2; in contrast, CH2 of chain 1 has an average B of 25 Å^2, and for CH2 of chain 2, the average B is 30 Å^2. These values demonstrate that in crystals of Fc fragment, the CH2 domains are less well ordered than the CH3 domains; CH2 of chain 2 is more disordered than CH2 of chain 1.

Bond lengths and bond angles of the refined model are very close to ideal values; the rms deviations are 0.007 Å and 1.7°, respectively. The rms deviation of ω and similar angles from minimum energy values if 5.9°. For the torsion angles which keep aromatic rings planar, the rms deviation is 1.8°.

An estimate of the accuracy of the refined Fc fragment coordinates can be obtained from comparison of chain 1 and chain 2. A total of 340 main-chain atoms from 85 residues of CH3 chain 1 with temperature factors below 35 Å^2 were rotated onto the corresponding atoms of chain 2. After least-squares refinement of the transformation parameters, the rms distance of equivalent atom positions was 0.29 Å. This

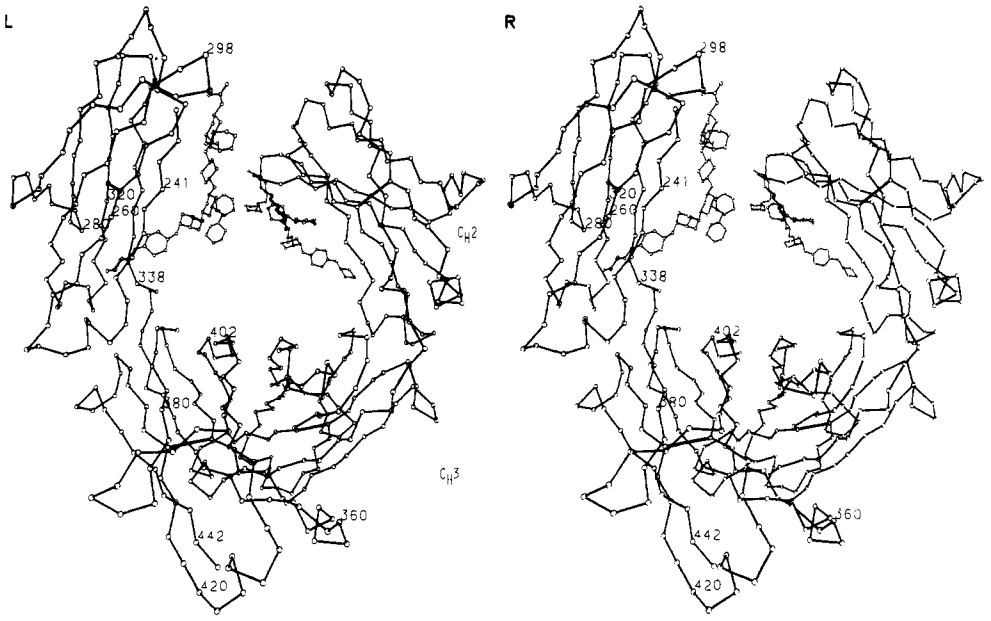

FIGURE 2: Stereo drawing of Fc fragment model (C^{α}) with carbohydrate (hexose rings, glycoside linkages, and Asn-297 side chain). Selected residues of chain 1 are labeled with residue numbers (residue numbering from myeloma protein Eu). Disulfide bridges are indicated by thick lines.

number is a rough estimate of the accuracy of coordinates which could be achieved in regions of high crystalline order. In regions with less order, the coordinate errors can be considerably larger. Such regions exist mainly in the CH2 domains. At 2.9-Å resolution carbonyl oxygens of the main chain cannot be located unambiguously in the electron-density map to determine the peptide orientations. This problem is less serious in regions with secondary structure. Outside these regions, especially in zones with high temperature factors, peptide orientations may be wrong even in the refined model.[2]

Crystallographic Refinement of FB–Fc Complex. The course of refinement of the FB–Fc complex model was very similar to that of Fc fragment and is briefly summarized here: The R value of the starting model was 0.40. Six cycles of real-space refinement using $2|F_{obsd}| - |F_{calcd}|$ maps calculated with model phases reduced the R value to 0.34. After additional cycles of Jack–Levitt refinement, the final R value was 0.24 for 6243 reflections between 7- and 2.8-Å resolution.[2] Energies and deviations of model parameters from ideal values are close to the values obtained for Fc fragment. Errors detected and corrected in the model of Fc fragment were corrected simultaneously in the Fc part of FB–Fc. To check these modifications and the model of the FB part, I inspected several $2|F_{obsd}| - |F_{calcd}|$ maps calculated with combined mir and model phases. Refinement of large parts of the CH2 domain and of parts of FB was hampered by poor crystalline order.

Description of Fc Fragment Model. Figure 2 shows a C^{α} drawing of Fc fragment, together with the attached carbohydrate chain. CH2 domains and CH3 domains are folded into two layers of antiparallel β-sheet structure which enclose a predominantly hydrophobic interior, a design typical for all immunoglobulin domains. The aggregation of CH3 domains is similar to that of the CH1–CL dimers in Fab fragments (Poljak et al., 1974; Segal et al., 1974; Matsushima et al., 1978; Marquart et al., 1980). The CH2 domains do not form a lateral contact with each other. Part of the CH2 C-contact face is covered by carbohydrate. The carbohydrate forms a weak bridge between CH2 domains.

Within the limits of error, the local symmetry axis relating CH3 domains is a diad. Expressed in polar angles, the rotational part of the transformation from CH3 chain 1 to CH3 chain 2 is $\varphi = 6.5$, $\psi = -100$, and $\kappa = -179.3$ (φ is the angle between the rotation axis and the y axis; ψ is the angle between the x axis and the projection of the rotation axis into the x–z plane; κ is the rotation angle). The loal symmetry axis relating CH2 domains with polar angles of $\varphi = 8.6$, $\psi = -100$, and $\kappa = -174.3$ differs from the CH3–CH3 axis by 2° in direction; the rotation angle differs by ~5° from a 2-fold rotation. In addition, the CH2–CH2 rotation is accompanied by a screw component of 1.1 Å. The differences between the local symmetries of CH2 and CH3 reflect flexibility in the CH2–CH3 contact region.

Table II (supplementary material) is a list of the possible hydrogen bonds between Fc fragment and carbohydrate. The table does not contain main-chain hydrogen bonds; these are shown in Figures 3 and 5.

CH2 Domain and Carbohydrate. Since the crystalline order is considerably better in CH2 chain 1 than in chain 2, the following description is based exclusively on the chain 1 model. The domain folding scheme with main-chain hydrogen bonds is shown in Figure 3. From the hydrogen bonding pattern, the layers of antiparallel β sheet can be clearly distinguished. Layer 1, which is equivalent to the C-contact face in CL, CH1, and CH3 domains, consists of four strands: Ser-239 to Phe-243, Thr-256 to Val-264, Lys-290 to Tyr-296, and Thr-299 to Leu-309. Layer 2 has three long strands: Lys-274 to Val-279, Glu-318 to Asn-325, and Ile-332 to Ile-336; residues Val-282 to Val-284 form a short piece of a fourth strand.

The carbohydrate moiety is attached to Asn-297 at the bend between strands 3 and 4 of layer 1. Figure 4 shows, in a series of three stereo drawings, the refined carbohydrate model and its position with respect to the CH2 domain; Figure 4c also shows the CH2 side chains involved in the contact. The CH2–carbohydrate contact is described in terms of the decrease of accessible surface area in Table III (supplementary material). The majority of buried CH2 residues are in strands

[2] Refined atomic coordinates of the Fc fragment and of the FB–Fc complex are available upon request. The coordinate sets also have been sent to the Protein Data Bank of Brookhaven National Laboratory, Upton, NY.

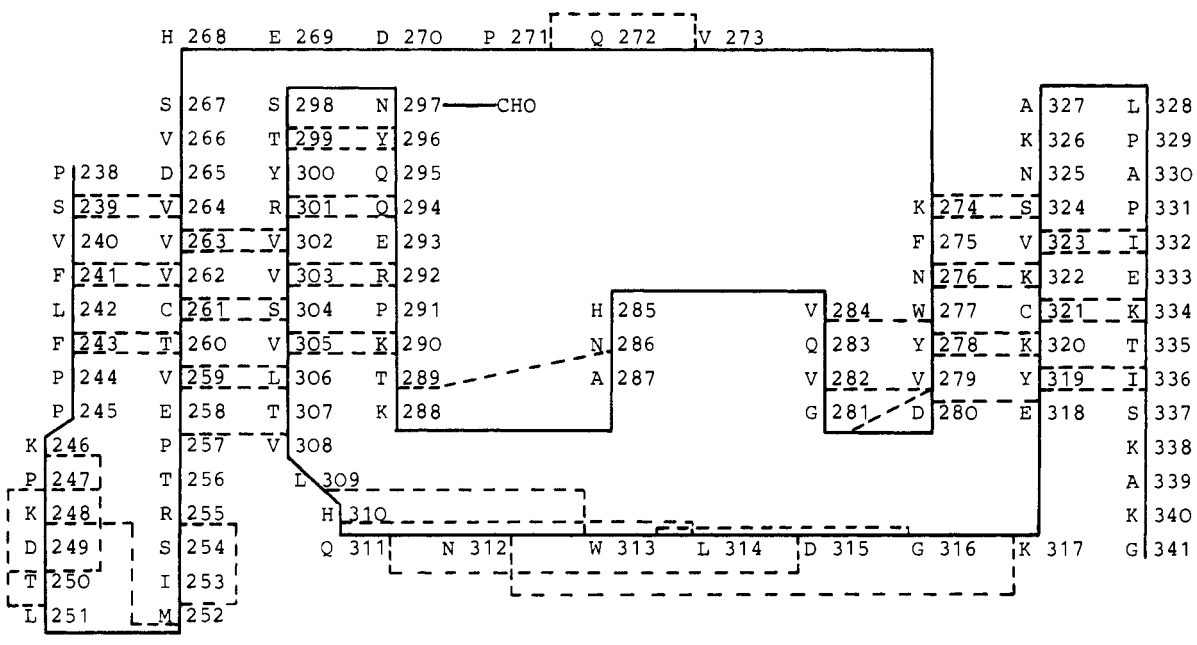

FIGURE 3: Schematic representation of chain folding (full line) and main-chain hydrogen bonds (dashed lines) of the CH2 domain. The one-letter code for amino acids is used.

1 and 2 of the C-contact face. Both hydrophobic and polar residues are involved. Six CH2 side chain atoms are within hydrogen-bonding distance to polar atoms of the carbohydrate; within the carbohydrate itself, six single additional hydrogen bonds are possible [Table II (supplementary material)]. Five of these are between adjacent hexose units: three between O3 and O5, one between O3 and O6, and one between O3 and O2. H bonds of this kind have been found in crystal structures of small polysaccharides [for a review, see Sundararajan & Marchessault (1979)]. With the exception of Asp-265, Asn-297, and Thr-299, the CH3 residues in structural positions analogous to the ones listed in Table III (supplementary material) are involved in the CH3–CH3 contact. This demonstrates that the carbohydrate in CH2 provides a substitute for the C–C contact and presumably helps to stabilize the CH2 domain. However, upon formation of the CH3–CH3 contact, about twice as much surface area [1090 Å^2; Table IV (supplementary material)] is covered per domain as in the CH2–carbohydrate contact (522 Å^2). This observation could explain the apparent "softness" of those parts of the CH2 domain which are most remote from the CH2–CH3 interface, which is indicated by large temperature factors or missing electron density. The difference of the temperature factors of CH2 chain 1 and chain 2 appears to be the result of different crystal environments: CH2 chain 1 is in contact with neighboring CH2 domains in the crystal at residues His-268, Lys-274, His-285, and Asn-297. In chain 2 these crystal contacts are missing; as a consequence, residues Val-266 to Asp-270, Gln-295 to Arg-301, and three hexose units (two *N*-acetylglucosamines and fucose) are disordered. The disorder in CH2 is even more pronounced in crystals of the FB–Fc complex, where the CH2 domain also lacks crystal contacts. Partial disorder of the CH2 domain can therefore be expected in solution. However, in the presence of the Fab arms, the CH2 domain might become ordered if a suitable Fab–CH2 contact is formed in an intact IgG molecule.

CH3 Domain and Contacts CH3–CH3 and CH2–CH3. Figure 5 shows a schematic drawing of the CH3 polypeptide chain with main-chain hydrogen bonds. Four strands of antiparallel β sheet are part of the C-contact face: residues Gln-342 to Leu-351, Glu-362 to Tyr-373, Asn-390 to Leu-398, and Ser-403 to Asp-413. The β-sheet geometry is severely distorted at residues Pro-343, Pro-346, Gly-371, Pro-395, and Pro-396. In the second face of the molecule, β strands are formed by residues Ile-377 to Glu-382, Val-422 to His-429, and Tyr-436 to Leu-443. As in CH2, a fourth strand is formed by residues Gln-386 to Glu-388. Residue Pro-374 is a *cis*-proline; the homologous proline residues in CH1 and CL of Fab Kol (Marquart et al., 1980) and in CH1 of Fab New (Saul et al., 1978) were also reported to be in cis conformation.

The loss of accessible surface area of individual residues upon formation of the CH3–CH3 contact is listed in Table IV (supplementary material). A total of 2180 Å^2 of accessible surface area is covered in the CH3 module. Possible inter-CH3 hydrogen bonds or charge interactions are shown in Table II (supplementary material). Almost all the residues involved in the CH3–CH3 contact are in positions homologous to the ones which participate in the CH1–CL contact in Fab Kol (Marquart, 1980) and in Fab New (Saul et al., 1978). Exceptions are Gln-347, Asn-390, and Thr-393. The interdomain salt bridge between Glu-357 and Lys-370 [Table II (supplementary material)] has its homologous equivalent in both Fab Kol and Fab New.

The residues involved in the CH2–CH3 contact are listed in Table V (supplementary material). With an accessible surface area of 778 Å^2 covered, this contact has roughly one-third of the size of the CH3–CH3 contact. According to Beale & Feinstein (1976), Leu-251, the most important hydrophobic residue in the contact, is conserved in IgG of man, mouse, guinea pig, and rabbit, in human IgA, and in the CH3 domain of human IgE. In CH3 of human IgM, the homologous residue is Ile. Other highly conserved contact residues are Pro-247, Met-252, Lys-338, Pro-374, Asp-376, Ile-377, and Glu-430.

Polar interactions in the CH2–CH3 contact are listed in Table II (supplementary material). The salt bridge between Lys-338 and Glu-430 appears to be a characteristic component of this type of contact. Lys-338 is conserved in CH2 domains

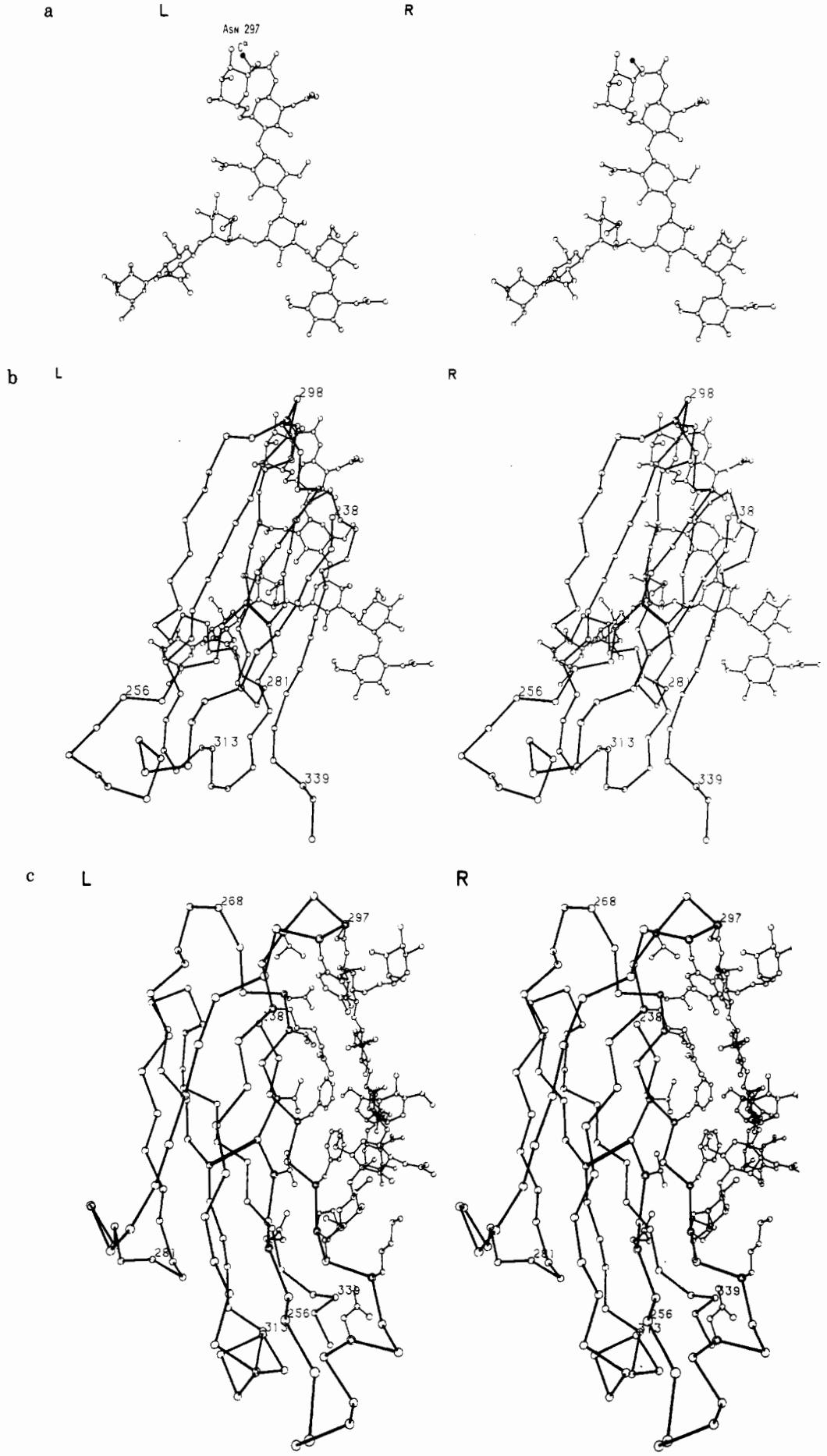

FIGURE 4: Stereo drawings of the carbohydrate and its interaction with the CH2 domain: (a) carbohydrate and side chain of Asn-297; (b) carbohydrate and C^{α} model of CH2 domain; (c) carbohydrate and C^{α} model of CH2 and CH2 side chains involved in the contact.

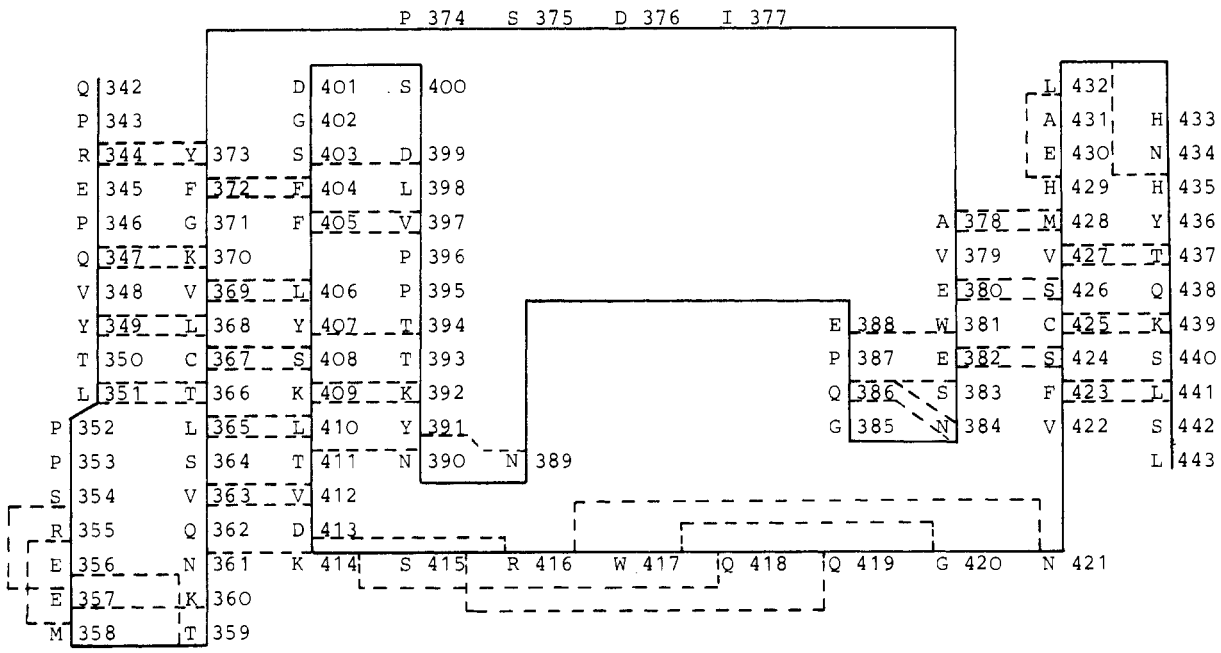

FIGURE 5: Schematic representation of chain folding (full line) and main-chain hydrogen bonds (dashed lines) of the CH3 domain. The one-letter code for amino acids is used.

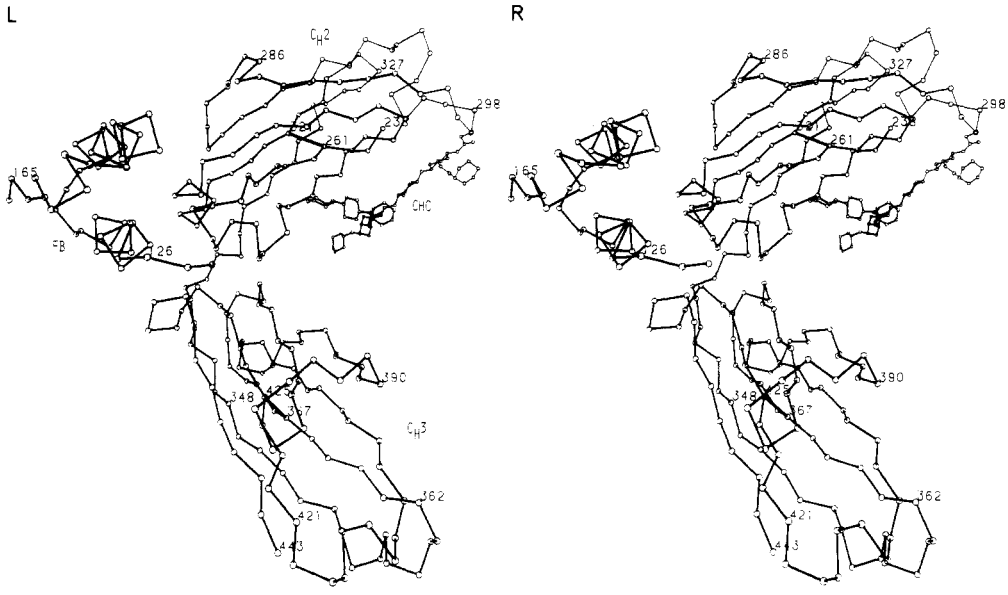

FIGURE 6: Stereo drawing of a monomer of the FB–Fc complex. Disordered regions in CH2 and in carbohydrate are indicated by reduced thickness of lines.

of IgG from man, mouse, guinea pig, and rabbit and in CH3 of human IgE; CH3 of human IgM has Arg instead of Lys. In human IgA, the homologous residue is Ser, but with Lys next to it. Glu-430 is conserved in CH3 of IgG and IgA and in CH4 of IgM and IgE; an exception is mouse IgG1 (MOPC 21), in which Gln was reported at this position. These sequence homologies indicate that the CH2–CH3 contact described here is very likely to be found in IgG and IgA and as a CH3–CH4 contact also in IgE and IgM.

FB–Fc Complex. Electron density for the FB part of the FB–Fc complex can be found from residues Phe-124 to Glu-166; residues Ala-120 to Lys-123 and Ala-167 to Lys-177 are disordered. Two antiparallel α helices formed by residues Gln-128 to Leu-136 and Glu-144 to Asp-155 are the predominant elements of secondary structure of FB. Table VI (supplementary material) shows the possible hydrogen bonds and charge interactions made by FB in the crystal. A large number of main-chain hydrogen bonds are typical for α helices. For residues Ser-158 to Glu-166, the electron density is weak and allows only the tracing of the polypeptide chain without giving information on peptide orientations.

FB makes two types of contact to symmetry-related Fc fragment chains in the crystal. Upon formation of contact 1, 1234 Å^2 of accessible surface area on FB and Fc is covered. As listed in Table VII (supplementary material), residues from CH2 and CH3 of Fc fragment and from the helical regions of FB are involved. Contact 1 is predominantly hydrophobic; only four hydrogen bonds between FB and Fc contribute to the stability of this contact [Table VI (supplementary material)].

The residues participating in contact 2 are shown in Table VIII (supplementary material). With 1012 Å^2 of accessible surface area covered, this contact is smaller than contact 1. Residues of the second helix and Asp-156 to Gln-159 of FB are covered. From the Fc fragment, only residues of the CH3 domain contribute to contact 2. In addition, a large peak of electron density near contact 2 was interpreted as a sulfate ion from the ammonium sulfate in the crystallization solution.

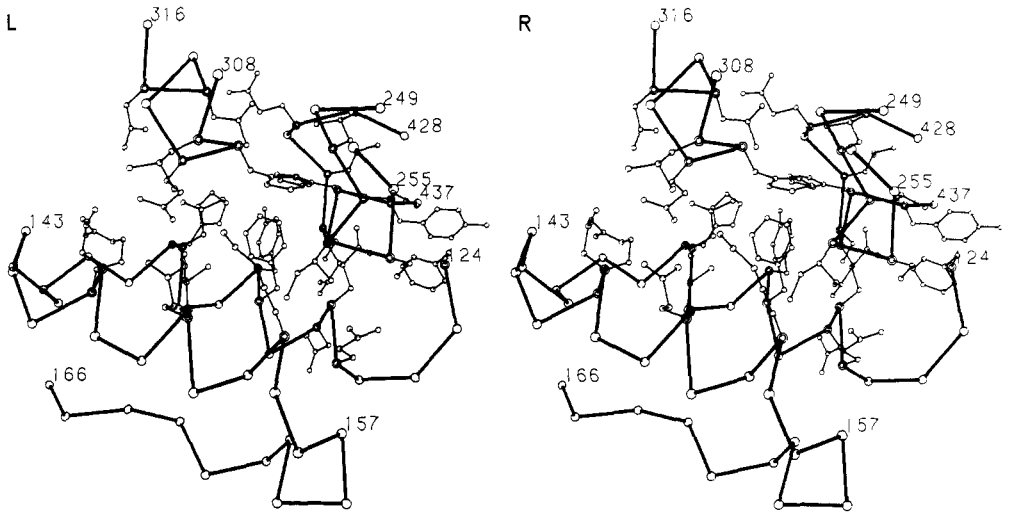

FIGURE 7: Stereo drawing of FB–Fc contact region with amino acid side chains. The course of the main chain of FB and of parts of Fc is drawn in thick lines.

Its negative charges are compensated by Lys-154 of FB and by Arg-416 of Fc. Including the sulfate ion, 14 hydrogen bonds or charge interactions [Table VI (supplementary material)] are observed in contact 2. Among these, the close proximity of Asp-155 of FB and Glu-388 of Fc, which are directly in the center of contact 2, is striking. FB–Bc crystals were grown at pH 4.1 (Deisenhofer et al., 1978); such a low pH appears to be necessary to allow Asp-155 and Glu-388 to be neighbors and the formation of contact 2. This observation and the contribution of a sulfate ion are strong arguments for the assumption that contact 2, although quite intimate, is a crystal contact. In solution, contact 2 should be possible only under conditions similar to the ones in the crystal.

Thus, under physiological conditions, it is most likely that only contact 1 can be formed in solution. Figure 6 shows a monomer of the FB–Fc complex with the molecules forming contact 1. The other half of the molecule is related to the one shown by an exact crystallographic diad. With the exception of small changes due to contact 2 at residues 384, 385, 388, and 416, the CH3 domain of FB–Fc is identical with CH3 in Fc fragment crystals. The CH2 domain of FB–Fc is even more disordered than the CH2 chain 2 of Fc fragment; residues Val-266 to Lys-274, Gln-295 to Tyr-300, and Asn-325 to Pro-331 and four hexose units of the carbohydrate are too mobile to be observed in the electron density. Since binding of protein A does not inhibit complement activation (Wright et al., 1977) and the binding site of C1q to Fc was reported to be on CH2 (Yasmeen et al., 1976), the C1q–Fc interaction must occur somewhere in the more mobile parts of CH2.

Figure 7 is a detailed picture of contact 1 between FB and Fc, including side chains. Ile-253 of Fc is totally covered by residues from FB. Other residues with a shielded area of more than 20 Å^2 are Met-252, Ser-254, Leu-309, His-310, Gln-311, Asn-434, His-435, and Tyr-436 of Fc and Phe-124, Gln-128, Gln-129, Asn-130, Phe-132, Tyr-133, Leu-136, Asn-147, Ile-150, Gln-151, and Lys-154 of FB [Table VII (supplementary material)].

As suggested previously (Deisenhofer et al., 1978), the inability of human IgG3 to form a complex with protein A (Michaelsen et al., 1977; Wolfenstein-Todel et al., 1976) can be explained by the substitution of Arg for His-435 in the Fc fragment. Model building with the display system showed that it is virtually impossible to find a place for the arginine in the complex. Close contacts would occur between the arginine side chain and residues Phe-132 and Leu-136 of FB and Leu-314 of Fc; in addition, the positive charge of the arginine would remain unbalanced. None of the other amino acid exchanges in CH3 of IgG3 (Michaelsen et al., 1977) are near contacts 1 or 2.

Acknowledgments

Discussions with Professor Robert Huber were helpful and stimulating throughout this work. Dr. T. A. Jones helped me to operate the interactive display system. Dr. W. S. Bennett made valuable suggestions which helped to improve the paper. The technical assistance of K. Epp during preparation of the drawings is acknowledged. I thank Drs. Robert Diamond, Michael Levitt, and the late Tony Jack for making their compter programs available to me.

Supplementary Material Available

Tables Ia and Ib (course of crystallographic refinement of Fc fragment), Table II (polar interactions in Fc fragment), Table III (CH2–carbohydrate contact), Table IV (CH3–CH3 contact), Table V (CH2–CH3 contact), Table VI (polar interactions of FB), Table VII (FB–Fc contact 1), and Table VIII (FB–Fc contact 2) (10 pages). Ordering information is given on any current masthead page.

References

Beale, D., & Feinstein, A. (1976) *Q. Rev. Biophys. 9*, 135.
Chothia, C. (1975) *Nature (London) 254*, 304.
Deisenhofer, J., & Steigemann, W. (1975) *Acta Crystallogr., Sect. B B31*, 238.
Deisenhofer, J., Colman, P. M., Huber, R., Haupt, H., & Schwick, G. (1976a) *Hoppe-Seyler's Z. Physiol. Chem. 357*, 435.
Deisenhofer, J., Colman, P. M., Epp, O., & Huber, R. (1976b) *Hoppe-Seyler's Z. Physiol. Chem. 357*, 1421.
Deisenhofer, J., Jones, T. A., Huber, R., Sjodahl, J., & Sjoquist, J. (1978) *Hoppe-Seyler's Z. Physiol. Chem. 359*, 975.
Diamond, R. (1966) *Acta Crystallogr., Sect. A A21*, 253.
Diamond, R. (1971) *Acta Crystallogr., Sect. A A27*, 436.
Diamond, R. (1974) *J. Mol. Biol. 82*, 371.
Hendrickson, W. A., & Lattman, E. E. (1970) *Acta Crystallogr., Sect. B B26*, 136.
Hermans, J., & McQueen, J. E. (1974) *Acta Crystallogr., Sect. A A30*, 730.
Hofmann, T., & Parr, D. M. (1979) *Mol. Immunol. 16*, 923.
Jack, A., & Levitt, M. (1978) *Acta Crystallogr., Sect. A A34*, 931.
Jones, T. A. (1978) *J. Appl. Crystallogr. 11*, 268.

Kornfeld, R., & Kornfeld, S. (1976) *Annu. Rev. Biochem. 45*, 217.
Lee, B., & Richards, F. M. (1971) *J. Mol. Biol. 55*, 379.
Levitt, M. (1974) *J. Mol. Biol. 82*, 393.
Levitt, M., & Lifson, S. (1969) *J. Mol. Biol. 46*, 269.
Marquart, M. (1980) Ph.D. Thesis, Technical University of Muenchen.
Marquart, M., Deisenhofer, J., Huber, R., & Palm, W. (1980) *J. Mol. Biol. 141*, 369.
Matsushima, M., Marquart, M., Jones, T. A., Colman, P. M., Bartels, K., Huber, R., & Palm, W. (1978) *J. Mol. Biol. 121*, 441.
Michaelsen, T. E., Frangione, B., & Franklin, E. C. (1977) *J. Immunol. 119*, 558.
Poljak, R. J., Amzel, L. M., Chen, B. L., Phizacherley, R. P., & Saul, F. (1974) *Proc. Natl. Acad. Sci. U.S.A. 71*, 3440.
Ponstingl, H., & Hilschmann, N. (1972) *Hoppe-Seyler's Z. Physiol. Chem. 353*, 1369.
Rutishauser, U., Cunningham, B. A., Bennet, C., Konigsberg, W. H., & Edelman, G. M. (1970) *Biochemistry 9*, 3171.
Saul, F. A., Amzel, L. M., & Poljak, R. J. (1978) *J. Biol. Chem. 253*, 585.
Schwager, P., Bartels, K., & Jones, T. A. (1975) *J. Appl. Crystallogr. 8*, 275.
Segal, D. M., Padlan, E. A., Cohen, G. H., Rudikoff, S., Potter, M., & Davies, D. R. (1974) *Proc. Natl. Acad. Sci. U.S.A. 71*, 4298.
Sjodahl, J. (1977) *Eur. J. Biochem. 78*, 471.
Steigemann, W. (1974) Ph.D. Thesis, Technical University of Muenchen.
Sundararajan, P. R., & Marchessault, R. H. (1979) *Adv. Carbohydr. Chem. Biochem. 36*, 315.
Wolfenstein-Todel, C., Frangione, B., Prelli, F., & Franklin, E. C. (1976) *Biochem. Biophys. Res. Commun. 71*, 907.
Wright, C., Willan, K. J., Sjodahl, J., Burton, D. R., & Dwek, R. A. (1977) *Biochem. J. 167*, 661.
Yasmeen, D., Ellerson, J. R., Dorrington, K. J., & Painter, R. H. (1976) *J. Immunol. 116*, 518.

Immunological Comparison of Rat, Rabbit, and Human Microsomal Cytochromes P-450†

F. Peter Guengerich,* Philip Wang, Patricia S. Mason, and Margaret B. Mitchell

ABSTRACT: Antibodies were raised in rabbits to electrophoretically homogeneous cytochromes P-450 isolated from rat and human liver microsomes. These antibodies were used to compare various forms of rat, rabbit, and human cytochromes P-450 present in microsomes and in purified preparations by using double-diffusion analysis, immunoelectrophoresis, quantitative microcomplement fixation, competitive radioimmune assay, and inhibition of enzyme activity toward *d*-benzphetamine and benzo[*a*]pyrene. The results indicate that (1) at least some forms of cytochrome P-450 from the three species share certain common immunological determinants, (2) there are immunological differences between cytochromes P-450 isolated from the three species, (3) some immunological differences exist between cytochromes P-450 isolated from rats of different strains, (4) immunologically distinguishable forms of cytochrome P-450 exist within individual human liver samples, and (5) human liver samples obtained from different individuals contain immunologically different forms of cytochrome P-450. Quantitative microcomplement fixation techniques were used to assign immunological distances to different forms of rat, rabbit, and human liver microsomal cytochrome P-450. Cross-reactivity was observed in all systems tested, and the extent of immunological similarity was dependent upon the particular assay used.

Cytochrome P-450[1] serves a pivotal role as the terminal oxidase in a microsomal mixed-function oxidase system that catalyzes the metabolism of a great variety of xenobiotics as well as endogeneous compounds (Coon et al., 1977; Gillette et al., 1974). The hepatic enzyme has been purified to apparent homogeneity as judged by various criteria from rats (Guengerich, 1978; Ryan et al., 1979; West et al., 1979), rabbits (Coon et al., 1978; Imai & Sato, 1974; Johnson & Muller-Eberhard, 1977; Kawalek et al., 1975; Philpot & Arinc, 1976), and mice (Huang et al., 1976). A large body of evidence has been accumulated which suggests that multiple forms of P-450 exist in experimental animals and that some are inducible [for reviews, see Guengerich (1979) and Lu (1979)]. Different animal species appear to contain different subsets of P-450s. This multiplicity appears to be important in the regulation of the types of P-450-mediated reactions carried out in a given individual (Coon et al., 1977).

Wide variation of carcinogen-metabolizing activities attributed to P-450 has been observed in human samples (Harris et al., 1979; Sabadie et al., 1980). Extension of the knowledge of P-450s in humans had been hampered by technical diffi-

† From the Department of Biochemistry and Center in Environmental Toxicology, Vanderbilt University School of Medicine, Nashville, Tennessee 37232. *Received May 2, 1980; revised manuscript received September 2, 1980.* This work was supported in part by Grants ES 01590 and ES 00267 and Contract NCI NO 1 CP 85672 from the U.S. Public Health Service.

* Address correspondence to this author. He is a recipient of Research Career Development Award ES 00041 from the U.S. Public Health Service.

[1] Abbreviations used: P-450, liver microsomal cytochrome P-450; C′, complement; Tris, 2-amino-2-(hydroxymethyl)-1,3-propanediol; EDTA, (ethylenedinitrilo)tetraacetic acid; RIA, competitive radioimmune assay; IgG, immunoglobulin G fraction; PB, phenobarbital; 3MC, 3-methylcholanthrene; BNF, β-naphthoflavone (5,6-benzoflavone); $NaDodSO_4$, sodium dodecyl sulfate; M_r, apparent monomeric molecular weight as determined by $NaDodSO_4$–polyacrylamide gel electrophoresis.

0006-2960/81/0420-2370$01.25/0